Journal of Alloys and Compounds 509 (2011) 7395–7399

Contents lists available at ScienceDirect

Journal of Alloys and Compounds

journal homepage: www.elsevier.com/locate/jallcom

Room-temperature flow in a metallic glass – Strain-rate dependence of shear-band behavior

W.H. Jiang[a,1], M. Atzmon[a,b,*]

[a] Department of Nuclear Engineering and Radiological Sciences, The University of Michigan, Ann Arbor, MI 48109, United States
[b] Department of Materials Science and Engineering, The University of Michigan, Ann Arbor, MI 48109, United States

ARTICLE INFO

Article history:
Received 4 January 2011
Received in revised form 1 April 2011
Accepted 5 April 2011
Available online 17 April 2011

Keywords:
Metallic glasses
Mechanical properties

ABSTRACT

The rate dependence of serrated flow in amorphous $Al_{86.8}Ni_{3.7}Y_{9.5}$ has been investigated by nanoindentation. Three samples, containing different initial amounts and distributions of free volume, were used: as quenched, cold rolled and annealed below the crystallization temperature. When the cold-rolled sample is indented at low rates, no new shear bands form, and stable, time-dependent, flow takes place at pre-existing shear bands, well below the glass transition temperature. Aside from instrumental resolution, factors that likely affect serrated flow include the magnitude of the yield drop and the shear-band propagation velocity. The trends we observe are compared with calculations based on the free-volume theory.

1. Introduction

At high strain rates and low temperatures, plastic deformation of metallic glasses is localized to narrow shear bands. This behavior has been attributed to a shear instability due to softening, caused by shear dilatation. Much of the research activity in this area was stimulated by Spaepen's pioneering treatment [1], in which he expressed the constitutive law in terms of the amount of free volume. While alternative models have been proposed (see, e.g., Ref. [2]), the Spaepen model has been useful in describing a range of behaviors, from Newtonian flow at low strain rate and high temperature, to strain localization and shear-band formation at the other extreme. The model was given additional microscopic content by Argon, who described the flow defects as shear transformations [3]. According to Spaepen's model, the strain-rate sensitivity of the stress required to activate a shear band is small, and that of the steady-state flow stress is even smaller [4]. Shear-band formation was modeled [3,4] by assuming the existence of "weakened bands" with higher free-volume content than their surroundings, at which the instability nucleates. Once a shear band forms, failure can result without any plastic deformation of adjoining regions. Under geometric constraints, e.g., indentation, rolling or compressive deformation of a sample with an appropriate aspect ratio, catastrophic failure is prevented and multiple shear bands can form.

Schuh et al. [5] observed serrated flow in nanoindentation of a metallic glass, the amplitude of which decreased, and the frequency of which increased, with increasing strain rate. At the highest rates used, no serrations were observed. Serrated flow has been attributed to the formation of shear bands [6], but serrations have also been shown to result from repeated activation of a single shear band [7]. We have reproduced in an Al-rich metallic glass the trends observed by Schuh et al., and observed, using atomic-force microscopy, that the number of shear bands that intersect the surface increased with increasing indentation rate [8]. We argued that, as the surface-step height decreased with increasing number of shear bands, it became increasingly difficult to resolve the formation of individual bands. In addition, the number of data points per unit depth may be too small at high rates to resolve serrations. Schuh et al. [9] later expanded their study and reported on serrated-flow behavior as a function of temperature and strain rate. They argued that serrated flow ceases when multiple shear bands form simultaneously, and demonstrated consistency of this argument with Argon's theory of flow localization [3]. A recent review of the current state of understanding of plasticity in metallic glasses is given in Refs. [10,11].

We have recently investigated the effect of cold rolling on the indentation response of $Al_{86.8}Ni_{3.7}Y_{9.5}$ at a loading rate of 0.5 mN/s [12]. The hardness of a rolled sample was lower than in the as-quenched state. Unlike the as-quenched sample, the rolled sample exhibited negligible serrated flow, and no pileups were observed near the indents. Annealing of the rolled sample led to a recovery of serrated flow and pileup, and to hardness values exceeding those of the as-quenched sample. We argued that deformation of the rolled sample took place by propagation of existing

* Corresponding author. Tel.: +1 734 764 6888; fax: +1 734 763 4540.
E-mail address: atzmon@umich.edu (M. Atzmon).
[1] Present address: Smith International, Inc., Houston, TX, United States.

0925-8388/$ – see front matter © 2011 Elsevier B.V. All rights reserved.
doi:10.1016/j.jallcom.2011.04.041

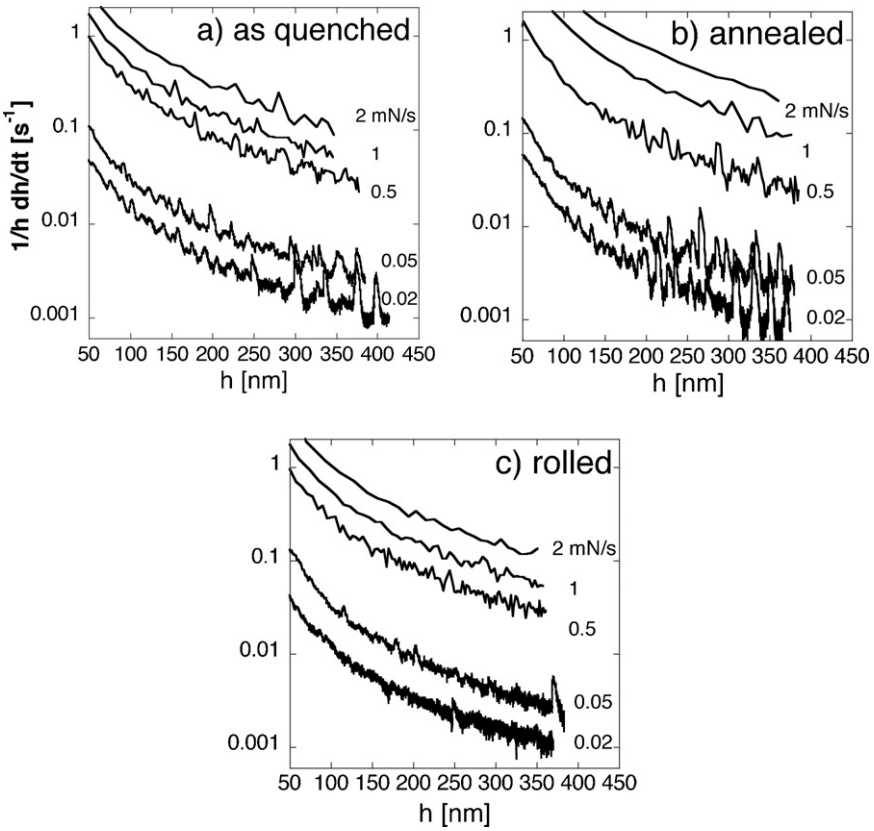

Fig. 1. Strain rates as a function of indenter depth for an as-quenched (a), an annealed (b) and a cold-rolled (c) sample for nanoindentation at varying loading rates.

shear bands, as opposed to nucleation and propagation of new shear bands in the as-quenched sample. In an effort to reach an improved understanding of shear-band behavior, we have performed a systematic investigation of the nanoindentation behavior of amorphous $Al_{86.8}Ni_{3.7}Y_{9.5}$ at room temperature at varying loading rates. The crystallization temperature of this alloy at a heating rate of 20 K/min is 275 °C [13], and it does not crystallize during shear-band formation at room temperature [14]. The state of the sample was varied by annealing or cold rolling. Although a significant temperature rise has been observed in shear bands, it is not the cause of their formation, but rather, its result [15,16]. Furthermore, the constrained geometry in the present work limits the displacement to less than 5% of that observed in Ref. [17], and thus limits the degree of adiabatic heating. Most notably, we observe time-dependent, stable, flow, at previously formed shear bands, a mode typically referred to as "homogenous flow" [1,3]. We explain some of the observed trends, using the free-volume-based approach [1,4].

2. Experimental details

An amorphous $Al_{86.8}Ni_{3.7}Y_{9.5}$ (at.%) ribbon, 22 μm thick and 1 mm wide, was obtained by the single-wheel melt-spinning technique using a Cr-coated Cu wheel at a tangential velocity of 40 m/s in vacuum. X-ray and electron diffraction analyses were employed to confirm the amorphous structure of the as-spun alloy ribbon. Samples were rolled in up to 100 small steps to a final thickness reduction of 45.5%. Relaxation anneals were carried out at 110 °C for 60 min in a Ti-gettered, flowing-Ar, furnace, a condition that does not lead to crystallization [12].

Samples were prepared for nanoindentation measurements by electropolishing from the wheel side of the ribbon, using a single-side jet thinning electropolisher for a few seconds. A solution of 25% nitric acid and 75% methanol was employed at 243 K and a voltage of 90 V. Load–displacement indentation curves and hardness values were obtained, using a Nanoinstruments Nanoindenter II with a Berkovich diamond indenter. The separation between adjacent indents was at least 20 μm. The loading phase was carried out under load control at loading rates ranging from 0.02 to 5 mN/s, to a maximum load of 10 mN. Atomic-force microscopy (AFM) observation on the indents was conducted using a Digital Instruments Nanoscope IIIa in contact mode.

3. Results and discussion

At low loading rates, the indentation data contain significant noise, which is especially noticeable in the indent-averaged strain rate, $\dot{\varepsilon} = (1/h)dh/dt$, where h is the indenter-tip displacement and t the time. In order to reduce the noise, $\dot{\varepsilon}$ vs. h curves were smoothed by convolution with a Gaussian. The width of this Gaussian in h was kept fixed for all curves, so as to preserve the trends in serration behavior. In Fig. 1, the strain rate is displayed as a function of indenter displacement for an as-quenched, a rolled and an annealed sample, for a range of loading rates. For the as-quenched sample, the serration amplitude decreases with increasing rate, as also previously reported [5,8]. Annealing clearly leads to more-pronounced serrations at loading rates of 0.5 mN/s and lower, but does not significantly affect their average frequency. Fig. 2 shows AFM images of indents in an as-quenched and an annealed sample, obtained at 0.5 mN/s. The annealed sample displays greater pileup volume and radius, and both samples display distinct surface steps.

For the rolled sample (Fig. 1c), a non-monotonic trend with loading rate is observed: the amplitude of serrated flow peaks at intermediated rates. Fig. 3 shows AFM images of indentations in the as-quenched and in the rolled sample, conducted at 0.02 and 2 mN/s each. At 0.02 mN/s, the rolled sample exhibits insignificant pileup or surface steps, whereas the as-quenched sample exhibits distinct surface steps due to shear bands. These steps have near-perfect circular arc shapes, whereas they are less regular for indentations formed at higher rate. At 2 mN/s, the pileup morphologies for the as-quenched and the rolled sample are very similar.

In the discussion below, the experimental results will be compared with idealized, one-dimensional, model calculations of

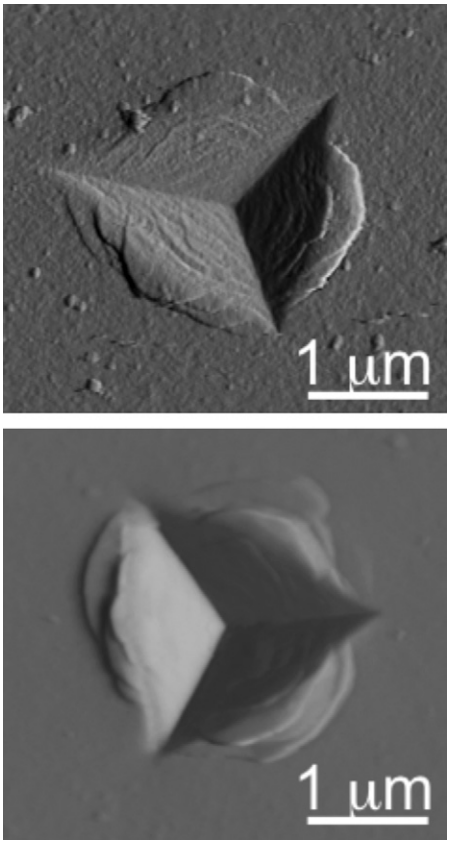

Fig. 2. AFM images of indents formed at 0.5 mN/s and a maximum load of 10 mN in an as-quenched (top) and an annealed sample (bottom).

stress–strain curves following Steif et al. [4] These calculations do not consider the complicated 3-dimensional stress distribution introduced by indentation. They are useful, however, in assessing the observed qualitative trends and pointing at the need for detailed 3-D computations, which are beyond the scope of the present work. An indentation-size effect [18] on the hardness is not expected to affect the qualitative trends we observe.

The analysis of Steif et al. [4] is based on two coupled differential equations: one describes the temporal derivative of the average free volume, $\bar{v}_f$, as a function of applied shear stress, $\bar{\tau}$:

$$\dot{\bar{v}}_f = v^* \nu_G \exp\left[-\frac{\alpha v^*}{\bar{v}_f}\right] \exp\left[-\frac{\Delta G_m}{kT}\right] \left\{\frac{2\alpha kT}{\bar{v}_f \bar{S}} \left(\cosh\frac{\bar{\tau}\Omega}{2kT} - 1\right) - \frac{1}{n_D}\right\} \quad (1)$$

where ν_G is the frequency of attempted jumps, the first exponent expresses the fraction of sites with free volume exceeding a critical value, v^*, required for atomic jumps to be feasible, and α is a geometric factor of the order of one that accounts for overlap of the free volume associated with individual atoms [19]. ΔG_m is the activation free energy for migration, kT has its usual meaning, and $\bar{S} = (2/3)\bar{G}(1+\nu)/(1-\nu)$, $\bar{G}$ being the shear modulus and ν, Poisson's ratio. $\bar{\tau}$ is the shear stress, n_D is the number of atomic jumps required to annihilate a free volume of v^* and Ω is an atomic volume. It should be noted that in later treatments, Ω is interpreted as the product of the volume and transformation strain of a *shear transformation zone* [3,20]. Eq. (1) is a simplistic treatment of free-volume annihilation process, and modifications to it have been proposed [21,22], but it suffices for the present qualitative discussion.

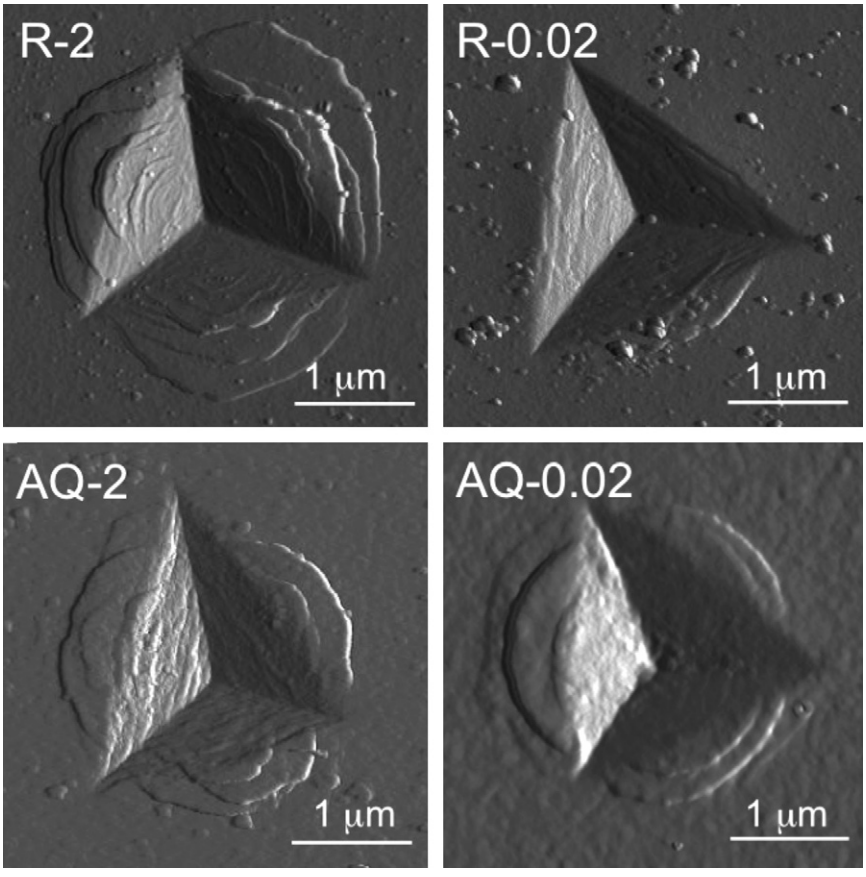

Fig. 3. AFM images of an as-quenced (AQ) and a rolled (R) sample, indented at 2 and 0.02 mN/s, as indicated.

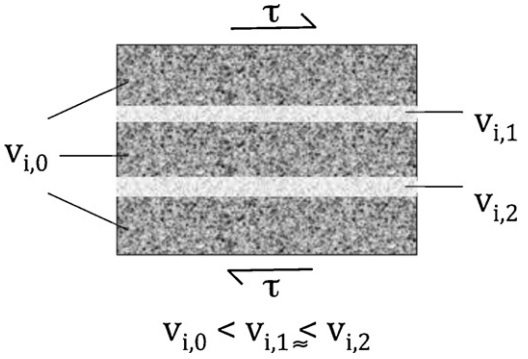

Fig. 4. The slab geometry used for a one-dimensional simulation of two parallel shear bands, following the simulation of a single shear band in Ref. [4].

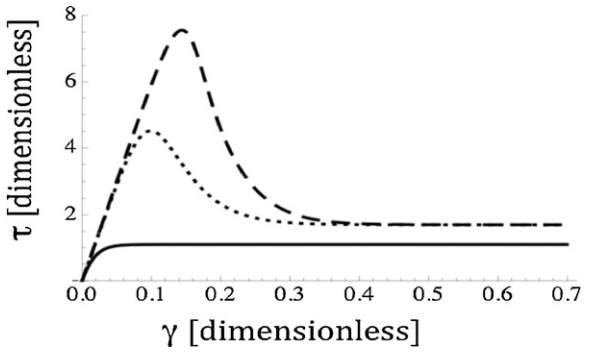

Fig. 5. Dimensionless stress–strain curves, calculated following Steif et al. [4], for initial free volume values, v_i, of 0.05 (solid line), 0.06 (dotted line) and 0.08 (broken line).

The second equation used by Steif et al. is the free-volume-dependent constitutive law:

$$\dot{\gamma} = \frac{\dot{\bar{\tau}}}{\bar{G}} + 2\nu_G \quad \exp\left[-\frac{\alpha v^*}{\bar{v}_f}\right] \exp\left[-\frac{\Delta G_m}{kT}\right] \sinh\left(\frac{\bar{\tau}\Omega}{2kT}\right) \tag{2}$$

where γ is the shear strain and $\dot{x}$ is the temporal derivative of variable x. For a fixed, externally imposed, strain rate, Steif et al. solved Eqs. (1) and (2) simultaneously and obtained the shear stress as a function of strain. As discussed below, their solution displayed linear behavior, followed by an abrupt and substantial yield drop once free-volume generation became significant.

In an attempt to explain the trend in strain-rate dependence of the shear-band spacing, we have performed a numerical calculation of the stress–strain curve for a slab subjected to a constant shear strain rate (Fig. 4). The slab contains two parallel "weakened zones," with slightly different initial amounts of free volume, v_i, both slightly higher than in the matrix. In this 1-dimensional model, the bands and the matrix deform in series. This is an extension of the calculation by Steif et al. for a single shear band [4]. At low strain rates, when v_i values in the two bands are sufficiently close, both bands experience similar strain. With increasing applied shear strain rate, one observes increasingly preferential straining of the band with the higher v_i value. This suggests that the number of shear bands would increase with increasing strain rate. This one-dimensional result is consistent with the trend observed in uniaxial compression [7]. However, it is opposite to the presently observed trend of increasing number of shear bands with increasing indentation strain rate. Our preliminary finite-element simulations of nanoindentation in three dimensions [23], also based on Ref. [4], show the same trend as in the present experiments, indicating that it is due to the 3-D geometry. We note that in addition to a description of the microscopic processes involved in shear-band nucleation, a complete understanding of shear-band formation would require a continuum-mechanical treatment of shear-band nucleation and propagation.

Fig. 5 shows calculated, dimensionless, shear stress–shear strain curves in one dimension for a fixed, dimensionless, strain rate of 10^{-5} and several values of v_i. Following Ref. [4], using its notation, the following parameters were used: a dimensionless shear modulus $G = \bar{G}\Omega/2kT = 60$; $\alpha = 1$; $\beta = 2(1+\nu)/3(1-\nu)\cdot v^*/\Omega = 1.2$ [24]. As expected, the magnitude of the yield drop, i.e., the difference between the peak stress and its steady-state value, increases with decreasing v_i. For the highest value of v_i, no yield drop is obtained and homogeneous flow is expected (see discussion below). When the curve displays a yield drop, one expects a shear band to form at the onset of instability, when the peak stress is exceeded in a sufficiently large region [25]. For a perfectly rigid loading frame, the resulting relaxation of the accumulated elastic stress is expected to lead to a drop in stress at fixed strain rate, or jump in indentation depth at fixed loading rate. The magnitude of these jumps is expected to be proportional to the yield drop, and consequently to increase with decreasing v_i, and therefore with annealing. The observed increases of serration amplitude, Fig. 1, and of the pileup and surface-step height, Fig. 2, with annealing, are both consistent with this argument since v_i decreases with annealing. For a quantitative analysis, the complicated indentation geometry would necessitate detailed 3-D numerical modeling.

In Fig. 6, the calculated peak stress is plotted as a function of strain rate for several initial values of the free volume, v_i. For each value of v_i, there is a threshold strain rate, below which the stress reaches a plateau with increasing strain, without a yield drop. Similarly, for a fixed strain rate, there is a threshold value of v_i, above which the yield drop vanishes (see Fig. 5). Beyond the threshold, the pre-existing free volume is sufficient to maintain the strain rate imposed. For this regime, the plateau stress value is used in Fig. 6. For each curve, the slope increases with decreasing strain rate, reaching a value of one, i.e., the flow becomes Newtonian [1], below the threshold strain rate. Above the threshold, shear-band formation is expected if the free-volume created remains localized on the time scale of the experiment. De Hey et al. [22] observed homogeneous deformation above this threshold, probably due to sufficiently rapid diffusion of the free-volume as it is created at the elevated temperature of the experiment. In Fig. 6, the locus of the threshold points is indicated for the different curves. A feature that

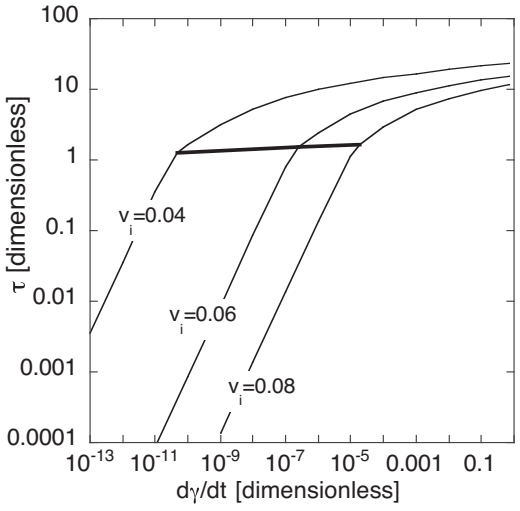

Fig. 6. Maximum stress (see Fig. 4) as a function of strain rate for several values of the initial free volume, v_i. The thick line denotes the locus of threshold points, at which the yield drop vanishes.

is crucial for the discussion below is that the threshold strain rate increases dramatically with increasing v_i values.

The maximum possible value of v_i in a glass has generally been considered to be limited by the quenching rate. However, the following discussion establishes that pre-existing shear bands are "weak links" at low strain rates, implying that the value of v_i in them is higher than in the typical rapidly quenched state. Fig. 6 shows that, at low strain rates, the stress is extremely sensitive to v_i. Therefore, the shear bands have a significantly lower viscosity than the matrix at low strain rates. Consequently, flow in the rolled sample takes place in the shear bands, well within the regime previously termed "homogeneous flow:" [1,3] flow is expected to be localized to shear bands because of their higher pre-existing value of v_i. This explains why no new shear bands nucleate, and no pileup is observed. Although shear bands formed by rolling are not arranged efficiently for deformation by nanoindentation, their drastically lower viscosity at low rates makes them the preferred deformation sites. In preliminary experiments, we have indeed directly observed room-temperature viscous flow at individual shear bands in this alloy [26]. At high loading rates, the viscosity of the pre-existing shear bands is closer to that of the undeformed matrix (Fig. 6) and, because of their inefficient geometry, they do not provide viable deformation paths. New shear bands nucleate, resulting in pile-ups and serrations (Fig. 3). At yet higher loading rates, the effect of shear band-nucleation and propagation becomes less visible in the indentation curves, as is also the case in the as-quenched sample, and as discussed in Refs. [5,8,9].

We note that the present discussion only addresses the qualitative trends observed. The load–displacement curves are affected by the complex deformation geometry, and by the average effect of many shear bands. Variations of the average stress we observe for different sample histories and indentation conditions are at most 25%, whereas the calculated local variations are much greater. This is not surprising, considering that the shear bands (i) occupy a small volume fraction of the sample; and (ii) can nucleate at local stress concentrations well before the peak stress (Fig. 5) is reached macroscopically.

Shear bands are expected to form during nanoindentation at a point at which the shear stress exceeds the local yield point in a sufficiently large region [25]. Although the local maximum stress in a homogeneous solid is obtained along a smooth curve [27], irregular distribution of the free volume might lead to an irregular shape of the shear band as it propagates along a path of least resistance. If the relative sensitivity of the yield stress to the amount of initial free volume, v_i were to increase with strain rate, it would explain the fact that the shear bands are circular at low strain rates only. However, we find that both analytical and numerical results, based on Steif et al. [4] display the opposite trend. One could argue that a perfect circular shape is obtained if the shear bands propagate laterally on a time scale that is significantly shorter than that for the expansion of the stress field. However, based on our preliminary finite-element simulations [23], this is not the case. This suggests, again, that more attention needs to be given to the 3-D continuum mechanics of shear-band nucleation and propagation.

4. Summary

In a cold-rolled metallic glass, low-rate indentation is accommodated by pre-existing shear bands. With increasing loading rate, the behavior resembles that of the as-quenched material, and new shear bands form. This observed trend is explained in terms of a free-volume based approach. Due to the high amount of residual free volume trapped in the shear bands after their formation, they can exhibit stable, time-dependent, flow during low-rate, room-temperature nanoindentation. A full theory of shear-band behavior would need to account for the atomistic and continuum-mechanics aspects of their nucleation and propagation in 3 dimensions.

Acknowledgements

We thank Dr. F. Pinkerton for providing the sample used in this study, and Prof. F. Spaepen for useful discussions. This work was funded by the US National Science Foundation (NSF), Grants DMR-0314214 and DMR-0605911.

References

[1] F. Spaepen, Acta Metall. 25 (1977) 407.
[2] T. Egami, J. Alloys Compd. 434–435 (2007) 110.
[3] A.S. Argon, Acta Metall. 27 (1979) 47.
[4] P.S. Steif, F. Spaepen, J.W. Hutchinson, Acta Metall. 30 (1982) 447.
[5] C.A. Schuh, T.G. Nieh, Y. Kawamura, J. Mater. Res. 17 (2002) 1651.
[6] W.J. Wright, R.B. Schwarz, W.D. Nix, Mater. Sci. Eng. A 319–321 (2001) 229.
[7] W.H. Jiang, G.J. Fan, F.X. Liu, G.Y. Wang, H. Choo, P.K. Liaw, J. Mater. Res. 21 (2006) 2164.
[8] W.H. Jiang, M. Atzmon, J. Mater. Res. 18 (2003) 755.
[9] C.A. Schuh, A.C. Lund, T.G. Nieh, Acta Mater. 52 (2004) 5879.
[10] C.A. Schuh, T.C. Hufnagel, U. Ramamurty, Acta Mater. 55 (2007) 4067.
[11] M.M. Trexler, N.N. Thadhani, Prog. Mater. Sci. 55 (2010) 759.
[12] W.H. Jiang, F.E. Pinkerton, M. Atzmon, Acta Mater. 53 (2005) 3469.
[13] Y. He, G.J. Shiflet, S.J. Poon, Acta Metall. Mater. 43 (1995) 83.
[14] W.H. Jiang, F.E. Pinkerton, M. Atzmon, J. Mater. Res. 20 (2005) 696.
[15] J.J. Lewandowski, A.L. Greer, Nat. Mater. 5 (2006) 15.
[16] Y. Zhang, A.L. Greer, Appl. Phys. Lett. 89 (2006) 071907.
[17] K. Georgarakis, M. Aljerf, Y. Li, A. LeMoulec, F. Charlot, A.R. Yavari, K. Chornokhvostenko, E. Tabachnikova, G.E. Evangelakis, D.B. Miracle, A.L. Greer, T. Zhang, Appl. Phys. Lett. 93 (2008) 031907–31911.
[18] N. Van Steenberge, J. Sort, A. Concustel, J. Das, S. Scudino, S. Suriñach, J. Eckert, M.D. Baro, Scripta Mater. 56 (2007) 605.
[19] M.H. Cohen, D. Turnbull, J. Chem. Phys. 31 (1959) 1164.
[20] J. Ju, D. Jang, A. Nwankpa, M. Atzmon, J. Appl. Phys. 109 (2011) 053522.
[21] S.S. Tsao, F. Spaepen, Acta Metall. 33 (1985) 881.
[22] P. De Hey, J. Sietsma, A. Van den Beukel, Acta Mater. 46 (1998) 5873.
[23] D. Jang, M. Atzmon, unpublished results.
[24] In order to reproduce the results of Ref. [4], reported for $v_i = 0.01$, $v_i = 0.04$ had to be used.
[25] C.E. Packard, C.A. Schuh, Acta Mater. 55 (2007) 5348.
[26] A. Ganuza, J.D. Ju, M. Atzmon, unpublished results.
[27] R. Vaidyanathan, M. Dao, G. Ravichandran, S. Suresh, Acta Mater. 49 (2001) 3781.